

# Journal Pre-proof

Distinct early serological signatures track with SARS-CoV-2 survival

Caroline Atyeo, Stephanie Fischinger, Tomer Zohar, Matthew D. Stein, John Burke, Carolin Loos, Denise J. McCulloch, Kira L. Newman, Caitlin Wolf, Jingyou Yu, Kiel Shuey, Jared Feldman, Blake Marie Hauser, Tim Caradonna, Aaron Schmidt, Todd J. Suscovich, Caitlyn Linde, Yongfei Cai, Dan Barouch, Edward T. Ryan, Richelle C. Charles, Douglas Lauffenburger, Helen Chu, Galit Alter



PII: S1074-7613(20)30327-7

DOI: <https://doi.org/10.1016/j.immuni.2020.07.020>

Reference: IMMUNI 4428

To appear in: *Immunity*

Received Date: 22 May 2020

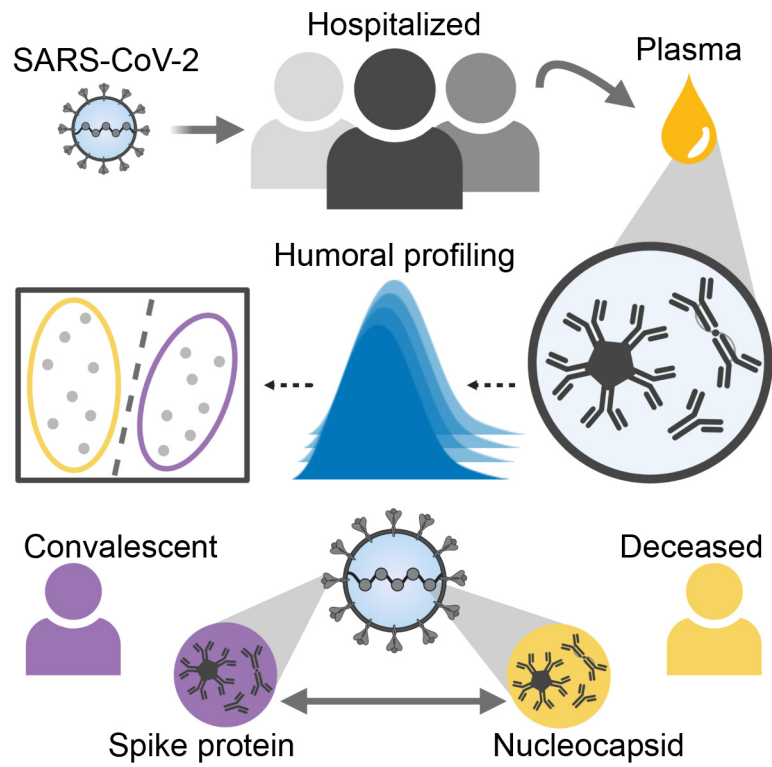
Revised Date: 29 June 2020

Accepted Date: 23 July 2020

Please cite this article as: Atyeo, C., Fischinger, S., Zohar, T., Stein, M.D., Burke, J., Loos, C., McCulloch, D.J., Newman, K.L., Wolf, C., Yu, J., Shuey, K., Feldman, J., Hauser, B.M., Caradonna, T., Schmidt, A., Suscovich, T.J., Linde, C., Cai, Y., Barouch, D., Ryan, E.T., Charles, R.C., Lauffenburger, D., Chu, H., Alter, G., Distinct early serological signatures track with SARS-CoV-2 survival, *Immunity* (2020), doi: <https://doi.org/10.1016/j.immuni.2020.07.020>.

This is a PDF file of an article that has undergone enhancements after acceptance, such as the addition of a cover page and metadata, and formatting for readability, but it is not yet the definitive version of record. This version will undergo additional copyediting, typesetting and review before it is published in its final form, but we are providing this version to give early visibility of the article. Please note that, during the production process, errors may be discovered which could affect the content, and all legal disclaimers that apply to the journal pertain.

© 2020 Published by Elsevier Inc.



## Distinct early serological signatures track with SARS-CoV-2 survival

Caroline Atyeo<sup>1,2,#</sup>, Stephanie Fischinger<sup>1,3,#</sup>, Tomer Zohar<sup>1,4,#</sup>, Matthew D. Stein<sup>1</sup>, John Burke<sup>1</sup>, Carolin Loos<sup>1,4</sup>, Denise J. McCulloch<sup>5</sup>, Kira L. Newman<sup>5</sup>, Caitlin Wolf<sup>5</sup>, Jingyou Yu<sup>6</sup>, Kiel Shuey<sup>5</sup>, Jared Feldman<sup>1</sup>, Blake Marie Hauser<sup>1</sup>, and Tim Caradonna<sup>1</sup>, Aaron Schmidt<sup>1</sup>, Todd J Suscovich<sup>8</sup>, Caitlyn Linde<sup>8</sup>, Yongfei Cai<sup>9</sup>, Dan Barouch<sup>6</sup>, Edward T. Ryan<sup>7</sup>, Richelle C. Charles<sup>7</sup>, Douglas Lauffenburger<sup>4</sup>, Helen Chu<sup>5\*</sup>, and Galit Alter<sup>1,10\*</sup>

<sup>1</sup> Ragon Institute of MGH, MIT, and Harvard, MA, Cambridge, USA

<sup>2</sup> PhD program in Virology, Division of Medical Sciences, Harvard University, Boston, MA, USA

<sup>3</sup> PhD program in Immunology and Virology, University of Duisburg-Essen, Essen, Germany

<sup>4</sup> Department of Biological Engineering, Massachusetts Institute of Technology, Cambridge, MA, USA

<sup>5</sup> Department of Medicine, University of Washington, Seattle, WA, USA

<sup>6</sup> Center for Virology and Vaccine Research, Beth Israel Deaconess Medical Center, Harvard Medical School, Boston, MA 02215, USA

<sup>7</sup> Infectious Disease Division, Massachusetts General Hospital, Boston, MA, USA

<sup>8</sup> SeromYx Systems, Cambridge, MA, USA

<sup>9</sup> Division of Molecular Medicine, Boston Children's Hospital, and Department of Pediatrics, Harvard Medical School, Boston, MA, USA

<sup>10</sup> Lead Contact

# These authors contributed equally to this work.

\*Corresponding authors:

Helen Chu: [helenchu@uw.edu](mailto:helenchu@uw.edu)

Galit Alter: [galter@partners.org](mailto:galter@partners.org)

**Summary:**

As SARS-CoV-2 infections and death counts continue to rise, it remains unclear why some individuals recover from infection whereas others rapidly progress and die. While the immunological mechanisms that underlie different clinical trajectories remain poorly defined, pathogen-specific antibodies often point to immunological mechanisms of protection. Here, we profiled SARS-CoV-2-specific humoral responses on a cohort of 22 hospitalized individuals. Despite inter-individual heterogeneity, distinct antibody signatures resolved individuals with different outcomes. While no differences in SARS-CoV-2-specific IgG levels were observed, spike-specific humoral responses were enriched among convalescent individuals, whereas functional antibody responses to the nucleocapsid were elevated in deceased individuals. Furthermore, this enriched immunodominant S-specific antibody profile in convalescents was confirmed in a larger validation cohort. These results demonstrate that early antigen-specific and qualitative features of SARS-CoV-2-specific antibodies, point to differences in disease trajectory, highlighting the potential importance of functional antigen-specific humoral immunity to guide patient care and vaccine development.

**Keywords:**

SARS-CoV-2, COVID-19 patients, SARS-CoV-2-specific antibody, functional antibody

**Introduction:**

SARS-CoV-2 is the newest coronavirus to cross into the human population (Wu et al., 2020b; Zhu et al., 2020). Millions of infections have been diagnosed (WHO, 2020); however, the number of asymptomatic carriers is likely to far exceed these numbers (Li et al., 2020). While the rapid spread of SARS-CoV-2, even during the asymptomatic phase of this infection, is alarming, more harrowing is our inability to predict disease trajectories among symptomatic individuals. In the absence of therapeutics and vaccines as countermeasures for this infection, there is an urgent need to begin to map the evolution of immunity to the pathogen to guide patient care and future immune interventions.

Although both antibody responses and T cells have been linked to disease resolution (Chen et al., 2020), and neutralizing antibodies have been demonstrated to block infection in small animal models (Quinlan et al., 2020), little is known about the antibody features that are important for protection. Neutralizing antibodies develop in the majority of SARS- and MERS-infected individuals (Chang et al., 2005; de Wit et al., 2016); however, the virus can mutate to overcome these antibody responses (He et al., 2006; ter Meulen et al., 2006). Passive immunization studies with both neutralizing and poorly neutralizing antibodies have shown protection in lethal MERS infection in mice (Zhao et al., 2015; Zhao et al., 2017), suggesting that both the neutralizing and extra-neutralizing functions of antibodies may play a critical role in control and resolution of disease. Moreover, recent studies have found lower neutralization titers in younger individuals and higher neutralization among individuals with severe disease (Wu et al., 2020a)(Wang et al., 2020), suggesting that antibodies may depend on additional mechanisms to clear the virus.

Antibody dynamics during the acute window of infection have been linked to differential outcomes across infections, including HIV (Tomaras and Haynes, 2009), influenza (Cobey and Hensley, 2017), and Ebola virus infection (Saphire et al., 2018). Specifically, the selection of specific antibody subclasses and functional profiles is heavily influenced by inflammatory cascades and may not only forecast disease outcomes but also point to antibody mechanisms of action vital in early pathogen control and clearance. However, whether identifiable antibody functional profiles across SARS-CoV-2 antigen-specificities evolve early following infection that track differentially with disease outcome is unknown. In this study, we assembled two cross-sectional sample sets of SARS-CoV-2-infected individuals at the time of hospital admission to begin to comprehensively profile the evolution of the early SARS-CoV-2 S-specific response and to define antibody features that are predictive of disease outcome. Through this analysis, we found that deceased and convalescent individuals present different

humoral profiles, with a more S-focused response in individuals who convalesced and a stronger N-specific response in individuals who succumbed to disease.

**Results:****Early SARS-CoV-2 antibody profiles in individuals that ultimately convalesce or pass away**

Across infectious diseases, pathogen-specific antibodies can serve as biomarkers of infection and aid in the early control and clearance of infection by blocking host-pathogen interactions and/or recruiting innate immune functions (Gunn and Alter, 2016). In order to investigate whether early SARS-CoV-2-specific humoral immune responses differ across individuals that ultimately recover or die from infection, a cohort of 22 hospitalized SARS-CoV-2-infected individuals, of whom 12 recovered and 10 died, was profiled. Samples were collected at hospital admission, all recruited within the first 20 days following symptom onset (**Table 1 and Figure S1**) at the University of Washington, Seattle, one of the earlier epicenters in the US (Holshue et al., 2020). Population demographics largely resemble those previously reported (Bhatraju et al., 2020), including elevated numbers of elderly men in the subset that died.

To profile the SARS-CoV-2-specific humoral immune response, we performed Systems Serology to determine the biophysical and functional characteristics of SARS-CoV-2-specific antibodies that recognize the SARS-CoV-2 spike (S), the S-derived receptor binding domain (RBD), and the nucleocapsid (N). The titers of SARS-CoV-2-specific isotypes and subclasses, the Fc $\gamma$ -receptor binding profiles, neutralization, as well as antigen-specific innate effector functions were measured. Heterogeneous responses were observed across both populations (**Figure 1A and Figure S2**), and convalescents did not appear to possess quantitatively superior immune responses that could explain their different later disease course. Univariate analyses further confirmed that no significant differences were observed in SARS-CoV-2-specific IgG1 or IgA1 titers across S, RBD, and N (**Figure 1B-C, and Figure S2**). Conversely, subtle distribution differences were observed for SARS-CoV-2-specific IgM responses, with a slight shift towards higher S-specific IgM among survivors, and a trend towards increased N-specific IgM responses among individuals who died (**Figure 1C**). Functional antibody profiles displayed similar distributions across the cohorts for antibody dependent cellular phagocytosis (ADCP) (**Figure 1D**) and neutralization (**Figure 1G**). Surprisingly, RBD-specific antibody-mediated NK cell degranulation (NKD) and antibody dependent neutrophil phagocytosis (ADNP), both driven through related Fc $\gamma$ -receptors Fc $\gamma$ R3A and Fc $\gamma$ R3B, respectively, trended towards increases among individuals who died (**Figure 1D-F**). Antibody measurements were minimally influenced by time since symptom onset (**Figure S1**), suggesting equivalent evolution of humoral immune responses across groups. However, no single antibody feature could discriminate between the groups.

### Differences in antibody profile coordination between groups

Beyond univariate differences, emerging data point to a critical role for humoral immune response coordination as a predictor of protection in some infections (Ackerman et al., 2018; Barouch et al., 2015). Given the polyclonal nature of the early humoral immune response, multiple functions or features may simultaneously contribute to differential control and clearance of infection. Correlation matrices split by group were used to examine the relationships between antibody isotypes or subclasses and antibody-dependent effector functions across the groups (**Figure 2A**). Within both groups, isotypes and subclasses were highly correlated. Conversely, the relationship between isotype or subclass and functions differed across the two populations. Stronger correlations between titers and functions were observed in convalescent individuals (**Figure 2A**). Disparities were observed in both NK cell and neutralizing antibody coordination between the two groups. Though not significant, individuals who died exhibited correlated isotype or subclass responses with monocyte and neutrophil phagocytosis, but negative and generally poorer correlations of NK cell activating and complement recruiting antibody responses with all other functions(**Figure 2A**), suggesting that individuals who pass away develop a functionally biased humoral immune response. While IgG1 responses were associated with all functions across the individuals that later went on to die, diversified isotype and subclass responses were largely inversely correlated with antibody-dependent complement deposition (ADCD) and natural killer cell (NK) NK functions. This observation suggests that these individuals leverage isotype and subclass diversification in a manner that may preclude the full deployment of the humoral immune response.

Conversely, convalescents overall displayed a more uniform correlation profile across subclass and isotype responses and antibody effector function. However, while neutralizing antibody responses were co-induced with isotype and subclass and effector functions among individuals who died, neutralizing antibody responses were largely inversely correlated to all antibody responses among individuals that went on to recover, suggesting a divergent evolution of the antigen-binding and constant domain of the antibody across these populations. These data highlight multiple early functional differences in SARS-CoV-2 specific humoral immunity between the groups.

To further probe the overall humoral profile between groups, the mean percentile of each antibody metric was determined across SARS-CoV-2-antigen specificities for both populations (**Figure 2B**). The nightingale rose plots reveal that deceased individuals exhibited a more N-focused humoral immune response compared to the S-centric response elicited among convalescents. In particular, higher S-specific ADCD, ADNP, ADCP and enhanced IgG1, IgA1, and IgM responses were observed among survivors. In contrast, S-specific NK cell activating responses were enriched in deceased.

Unexpectedly, RBD-specific responses were largely enriched among individuals that went on to pass away, with the exception of RBD-specific monocyte phagocytosis which was enriched among individuals that went on to survive. These data point to both antigen-specific and antibody-effector differences early in infection that differ by clinical trajectory.

### Defining signatures that differentiate disease trajectory

Given the unique correlation and immunodominance profiles across the groups (**Figure 2A and B**), we next aimed to define whether a minimal set of features could be identified that could segregate individuals with different clinical outcomes. To this end, feature down-selection was performed to avoid overfitting, followed by partial least squares discriminant analysis (PLSDA) to visualize differences (Lau et al., 2011). Despite the small numbers, separation was observed across the groups (**Figure 3A**). All antibody features as well as sex and interventions (**Table 1**) were included in the analysis, and as few as 5 features were sufficient to drive separation across the subjects (**Figure 3A and B**). S-specific IgM and IgA1 responses were enriched in survivors, whereas N-specific complement activity (ADCD), IgM, and IgA1 titers were enriched in individuals who died. These data likely relate to the immunodominant shift towards S in convalescent individuals and towards N in deceased individuals (**Figure 2B**). Model performance was evaluated using leave-one-out cross validation, to test that significance of the model using different sets of subjects and to test outlier effects. The model clearly outperformed (Cliff's  $\Delta$ ) permuted and size-matched random controls (**Figure 3C**). Moreover, sensitivity analysis, evaluating model performance with the removal of individual outliers, highlighted the minimal impact of any given individual (**Figure S3A**). Furthermore, individual model features only possessed modest predictive power in resolving the groups, but collectively, combining all 5 features -in Latent Variable 1 (LV1)- exhibited improved predictive accuracy (**Figure 3D**). Confounding features, such as days since symptom onset, sex, age, and viral load were also over-layed on the PLSDA scores plot (**Figure S3B-F**), highlighting the limited capacity of any of these features to distinguish individuals into those who convalesced or died. Furthermore, at individual levels, these demographic factors were poorly predictive of disease outcome, underperforming classification compared to the LV1 classification model (**Figure S3G**). Thus, a minimal set of SARS-CoV-2 humoral profiles, rather than demographic information, appear to significantly resolve individuals who later went on to die from those who recover.

Given that the feature down-selection algorithm selects a minimal set of features to avoid overfitting, a co-correlates network was used to explore additional features that may distinguish these two groups (**Figure 3F**). A larger set of co-correlates can help provide mechanistic clues related to the

immunologic mechanisms by which antibodies contribute to control and clearance of infection. Thus, a co-correlate network was built highlighting the relationship of model-selected features (large nodes) with additional highly correlated features (smaller nodes). Features enriched among individuals who later died, included N-specific IgM and IgA2, that were linked to a large number of additional N- and RBD-specific poorly functional antibody features. For example, correlates of risk were linked to the induction of less-functional IgG subclasses, IgG2 and IgG4, pointing to the early rise of dysregulated or less functional humoral immune responses as biomarkers or even drivers of ineffective control or clearance of infection. Conversely, S-specific IgM titers, enriched in convalescent individuals, were correlated with functional S-specific IgG3 responses, RBD-specific IgM, and S-specific monocyte and neutrophil phagocytosis. Moreover, S-specific IgA1 responses, also enriched among convalescents, were linked to RBD-specific complement activation (ADCD) and S-, RBD-, N-specific Fc $\gamma$ R2A binding, the Fc $\gamma$ -receptor involved in phagocytosis. Given our emerging appreciation for the role of complement and phagocytosis in vaccine mediated protection against SARS-CoV-2 (Yasui et al., 2014), these data potentially argue for a similar role for these functions in natural protection against disease. Moreover, the data also highlight the potential importance of a less N-focused, but more functional S-specific phagocytic response as an early correlate of recovery from infection.

#### **Validation of the skewed S-specific response in convalescents**

Collectively, the data point to a shift in immunodominance of spike versus nucleocapsid functional antibody responses. To test this hypothesis, we next compared the overall ratio of Spike(S):Nucleocapsid(N)-specific antibody isotype, subclasses, and functions across the groups (**Figure 4A and Figure S4A**). As expected, several antibody features were selectively biased towards S-immunity in the convalescents compared to individuals that later died, including IgM, ADCP, ADNP, and ADCD. Whether these effects were exclusive to this group of individuals from Seattle or could be generalized was next addressed in a second larger cohort of acutely infected individuals from Boston, of which 20 individuals convalesced and 20 died. Similarly, to the Seattle cohort, Boston samples were profiled in the first 20 days following symptom onset (**Table 2**). Similar to the Seattle discovery cohort, though differences were observed in S- and N-specific immune responses at a univariate level none passed multiple hypothesis correction (**Figure S4B**). Yet, when S:N ratios were compared across features, convalescent individuals exhibited a bias towards elevated S-specific humoral immunity compared to N-specific immunity in contrast to individuals who went on to later pass away (**Figure 4B and Figure S4C**). Thus, to ultimately capture the extent of S:N skewing across the groups, the number of features that

had greater S than N responses were summed across convalescents and deceased individuals and compared within each cohort (**Figure 4A and B**). In both cohorts, a significant enrichment of S:N immunity was observed in convalescents (**Figure 4C**). Therefore, these findings suggest that a consistent overall shift in S:N immunity early in SARS-CoV-2 infection may have a protective role and aid in recovery from severe disease.

**Discussion:**

Both cellular and humoral immune responses have been linked to protection against several coronaviruses (Li et al., 2006). Importantly, antibodies represent pathogen-specific markers of exposure, serve as powerful biomarkers of disease activity, and often point to immunological mechanisms of protection able to guide therapeutic or vaccine development (Gunn and Alter, 2016). By deeply profiling the SARS-CoV-2 humoral immune response early in infection, here, we defined a unique SARS-CoV-2-specific humoral signature associated with later disease outcomes. A combination of five SARS-CoV-2-specific antibody measurements were sufficient to distinguish individuals with different disease trajectories in a cohort from Seattle, including antibody measurements to S and N, with an overall enhanced S-centric response in individuals who recovered from infection. S-specific phagocytic and complement activity were enriched early in individuals that recovered from infection. This signature was confirmed in a second, larger SARS-CoV-2 infection cohort from Boston, where convalescent individuals exhibited a higher S:N ratio in their humoral immune response. These data point to early diverging humoral immune responses that may mark more effective immunity and suggest that functional antibodies directed against S might be beneficial for SARS-CoV-2 disease trajectory.

In SARS-CoV-1 and SARS-CoV-2 infection, N is highly immunogenic, with N-specific humoral immune responses arising concurrently with S-specific humoral immunity (Liu et al., 2020; Shi et al., 2004; Timani et al., 2004). However, immunization of hamsters with a vector expressing N offered no protection against SARS-CoV-2 challenge despite a strong anti-N response, whereas immunization with the same vector expressing S protected hamsters against challenge (Buchholz et al., 2004). It is estimated that 100 copies of S and 1000 copies of N are incorporated into each virion (Bar-On et al., 2020), suggesting that 10-fold more N may be produced compared to S during infection to effectively generate viral progeny. Due to the high amounts of nucleocapsid, N-directed responses may be indicative of higher disease burden and increased antigen exposure. However, the similarity in viral loads between the individuals who recovered and those who died does not support this hypothesis. Rather, the data point to compromised evolution of S-immunity in individuals that later pass away. The potential beneficial role of S-targeted immunity in viral control is reinforced in new studies in non-human primates (NHP), demonstrating elevated and robust functional humoral immune responses to S, rather than RBD and N, following primary infection that were associated with protection upon re-exposure to the virus (Chandrashekhar et al., 2020).

It is well known that timing of sampling may influence humoral profiles, where sampling time could result in the comparison of immature versus mature immune responses. Despite the sampling

differences in the group, comparable titers were observed across the convalescents and individuals that ultimately passed away. Moreover, similar overall functional profiles were also observed, suggesting that the humoral immune responses were comparable in magnitude across the two groups. Additional analysis of the influence of sampling time on the spread of the antibody profiles in the PLSDA highlighted a minimal influence of time from symptoms on overall antibody profile variation and the time of sampling exhibited a minimal predictive power in classifying individuals into convalescents or deceased. Yet, longitudinal analyses will be illuminating providing further information on the evolving humoral immune response that tracks with protection from infection.

Emerging data point to higher mortality among the elderly and across the genders (Hauser et al., 2020). Along these lines, individuals who passed away were on average older than those who convalesced. Age can have a profound effect on immune function, and though this study was not suited to explore the relationship between age, outcome, and humoral responses, future larger studies across age groups could provide insights on the differential susceptibility among the elderly. However, the impact of age, sex, and viral loads illustrated a minimal influence of each of these variables on the overall variability of the humoral immune responses. Additionally, the individual predictive power of these demographic variables were lower than the predictive power of the model selected antibody features (LV1).

While S-specific antibodies able to recruit NK cell activity were expanded in individuals that went on to pass away, pointing to a potentially negative influence of NK cells, coordination of NK and phagocytic activity was enriched among convalescents. These seemingly contradictory data point to the potential importance of synergy between innate immune effector functions. While NK cells have been implicated both in protection (Lu et al., 2016, Jegaskanda et al., 2016, van Erp et al., 2019) and pathology (Cong and Wei, 2019), it is possible that the evolution of antibodies able to harness the cytotoxic power of NK cells to eliminate infected or phagocytic cells may play a critical role in elimination and clearance of the infection. Interestingly, this coordination was associated with the synergistic evolution of a broader isotype and subclass specific response among convalescents. However, whether additional changes in antibody-Fc-glycosylation also contribute to this unique functionalization of antibody isotypes and subclasses, enabling coordination, remains unclear but could point to promising target immune profiles that may confer the greatest level of protection against the virus.

There are a number of limitations in this study. First, because these samples were collected early during the COVID-19 pandemic in the US, the Seattle study included a small number of participants, and the groups were not age or sex matched. Confounding factors such as timing of

sampling, sex and age are all known to influence SARS-CoV-2 infection and disease trajectory. While antibody profiles clearly segregated individuals that survived compared to that did not survive, more limited variation in antibody profiles were observed across age, sex, viral load and days from symptom onset. However, among the co-morbidities, age was the second major driver of variation in antibody profiles, pointing a potentially critical role for age-associated defects in Fc-variation that may contribute to altered antiviral immunity to SARS-CoV-2 and beyond. The larger validation cohort from Boston identified a similar humoral signature that discriminated survivors from non-survivors, highlighting the conserved nature of this immunological signature, independent of demographic characteristics. Whereas this study only attempted to understand the humoral disparities between convalescent and deceased individuals in a cohort of severely infected individuals, further studies may attempt to define humoral profiles able to further classify individuals across the clinical trajectory spectrum ranging from asymptomatic to severe disease.

Collectively, the data presented here argue for the evolution of distinct antigen-specific and functional humoral immune responses early in SARS-CoV-2 disease. While further analysis on longitudinal cohorts may provide further mechanistic insights on the specific role of antibodies in control and clearance of infection, here we validated an early functional humoral immune signature that appears to predict disease progression across two distinct cohorts. Linked to emerging animal model experiments, the correlates defined here may provide key mechanistic insights to guide therapeutic and vaccine design efforts.

### Acknowledgements

We thank Bruce Walker, Nancy Zimmerman, Mark and Lisa Schwartz, an Anonymous donor, and Terry and Susan Ragon for their support. We would also like to thank Bing Chen for protein production efforts. We acknowledge support from the Ragon Institute of MGH, MIT, the Massachusetts Consortium on Pathogen Readiness (MassCPR), and the Bill & Melinda Gates Foundation (235730), the NIAID (U19 AI35995) and the U.S. Centers for Disease Control and Prevention (CK000490).

**Author Contributions.** S.F., C.A., H.C., and G.A. designed the study. S.F., C.A., M.S., and J.B. performed the immunologic assays. H.C. collected and selected the clinical specimens. T.Z., C.L. and D.L performed all analyses. E.T.R. and R.C.C. participated in sample collection, study design and interpretation of data. A.G.S., J.F., T.C., B.M.H, and Y.C. provided purified proteins. G.A. wrote the paper with all co-authors.

**Declaration of Interests.** Galit Alter is a founder of SeromYx Systems.

**Correspondence.** Correspondence and requests for materials should be addressed to G.A. ([galter@partners.org](mailto:galter@partners.org)) and Helen Chu ([helenchu@uw.edu](mailto:helenchu@uw.edu)).

#### Main Figure Titles and Legends:

**Figure 1: Heterogeneity in antibody responses across SARS-CoV-2 antigens in individuals that recover or pass away.** 22 plasma samples from SARS-CoV-2 infected individuals were profiled at the time of hospitalization against SARS-CoV-2 S, RBD and N antigens. A: The heatmap shows the humoral immune responses across individuals that later passed away (deceased) or recovered (convalescent). The heatmap is split by SARS-CoV-2 S, RBD and N antigens. Rows correspond to individuals. Columns correspond to antibody features (background subtracted and z-scored) including neutralization, isotype, subclass, and antibody effector functions. High responses are shown in red and low responses are depicted in blue. B-G: Violin plots show the distribution of each antibody feature split across convalescent (purple) and deceased (orange) individuals across antigens. The dashed gray line indicates the median value of each distribution. A two sided Mann-Whitney U test was used to calculate uncorrected p- values, shown in the figure. No significance was detected after a Holm-Bonferroni correction for multiple hypothesis testing.

**Figure 2: Deceased Individuals show less coordinated and N-directed antibody responses.** A: The correlation heatmap shows pairwise spearman correlation matrices of antigen-specific antibody titers and effector functions for convalescent (left) and deceased (right) patients. For each feature analyzed, the bar covers the S, RBD, and N antigens, shown in the legend on the right. Statistical significance is indicated by gray asterisks with Holm-Bonferroni correction for multiple hypothesis testing ( $p<0.001$ ). Negative correlations are indicated in blue, and positive correlations are denoted in red. B: The nightingale rose plots show the mean percentile of antibody features within the deceased (top) and convalescent (bottom) groups. Plots represent the S, RBD, and N-specific responses across deceased (top) and convalescent (bottom) individuals. Each wedge represents a SARS-CoV-2 antibody feature. The size of the wedge depicts the magnitude of the value. The colors represent the type of feature: orange-antibody functions and purple-antibody isotypes and subclasses.

**Figure 3: Select antibody features distinguish convalescent and deceased individuals.** A: The PLSDA scores plot shows the degree of discrimination that was achievable across the groups following feature-down selection. Each dot represents an individual: convalescent (purple) and deceased (orange). Ellipses

correspond to the 95% confidence intervals for each group. B: The line graph shows the variable importance in projection (VIP) score of the selected features. As few as 5 features were required to separate the groups. The magnitude indicates the importance of the feature in driving separation in the model. The color of the feature corresponds to the group in which the feature is enriched. C: The violin plots show the distributions of repeated classification accuracy tests using the actual data, shuffled labels, and randomly selected size-matched features illustrating the performance and robustness of the model. Green squares indicate the median accuracies. D: The predictive power of the model built on the selected features is shown in the LV1 column. In addition, the predictive power of each individual selected feature is represented in grey. The predictive power is illustrated as the AUC of the ROC curves for the model (LV1) or each feature alone. E: The radar plot shows the z-scored univariate values of the selected features across both groups. F: The correlation network illustrates the co-correlated features (small nodes) that are significantly correlated with the Model-selected features (large nodes). Edge transparency corresponds to correlation strength. Antigens are indicated by different colors (S: teal, N: grey, and RBD: black).

**Figure 4. Converging shift in immunity across a second acute infection cohort.** The nightingale rose plots show the mean percentile of the Spike:Nucleocapsid (S:N) ratio of each read-out are depicted for the (A) Seattle or Discovery cohort and the (B) Boston or Validation cohort for the convalescents (left) and the deceased (right). Titers are shown as pink wedges and functions as blue wedges. (C) The whisker box plots show the number of S-features which are greater than their N-counterparts for all individuals in the Seattle or Discovery cohort (left) and the Boston or Validation cohort (right). Differences across the 2 groups were assessed using a one-sided Mann-Whitney U test.

#### Document S1: Figures S1-4

**Data S1: Source data of antigen specific titers, FcRs, and functional responses across samples.** Data includes raw values, sample descriptors, and data dictionary.

**Table 1: Demographics of SARS-CoV-2 cohort from Seattle**

<b>Characteristics</b>	<b>Convalescent (N=12)</b>	<b>Deceased (N=10)</b>
Female sex – no. (%)	4 (33.3)	3 (30)
<i>Age range - no. (%)</i>		
Younger than 49	3 (25)	1 (10)
50-59	4 (33.3)	0 (0)
60-69	4 (33.3)	2 (20)
70-79	0 (0)	4 (40)
80 and older	1 (8.3)	3 (30)
<i>Race or ethnic group – no (%)</i>		
Asian	2 (16.7)	1 (10)
Black	0 (0)	1 (10)
White	9 (75)	7 (70)
Missing Data	1 (8.3)	1 (10)
Median Days from Onset of Symptoms to Sample Collection (IQR)	13.5 (15-8)	7 (12-5)
Median Days Spent in ICU (IQR)*	13 (15-9)	13(14-9)
Median viral load (IQR)**	28.3 (30.4-26.5)	26.4 (28.375-21.725)
<i>Interventions - no./total no. (%)</i>		
Chloroquines	6/12 (50)	7/10 (70)
Remdesivir	9/12 (75)	7/10 (70)
Tocilizumab	3/12 (25)	0/10 (0)
Antibiotics	8/12 (66.7)	8/10 (80)
<i>Consequences of disease - no./total no. (%)</i>		
Acute respiratory distress syndrome	5/12 (41.7)	6/10 (60)
Non-ST-elevation myocardial infarction	1/12 (41.7)	5/10 (50)

\* For 4 of the deceased individuals' days from symptom onset was unknown

\*\*For half the recovered individuals viral load measurements were not available

**Table 2: Demographics of SARS-CoV-2 cohort from Boston**

<b>Characteristics</b>	<b>Convalescent (N=20)</b>	<b>Deceased (N=20)</b>
Female sex – no. (%)	6 (30)	6 (30)
Age (IQR)	56 (63-45)	78 (81.5-68)
Median Days from Onset of Symptoms to Sample Collection (IQR)	9 (14.25-7.5)	8.5 (12-6)

**STAR Methods:**

- Key Resource Table
- Resource Availability
  - Lead Contact
  - Material Availability
  - Data Availability
- Experimental model and subject details
  - Sample Set
  - Primary Immune Cells
  - Cell lines
- Method Details
  - Luminex
  - Functional Profiling
  - Pseudovirus Neutralization Antibody Assay
- Quantification and Statistical Analysis
  - Classification of Convalescent and Deceased Groups
  - Correlation Networks
  - Sensitivity Analysis
  - Ratio Based Analyses

**Resource Availability****Lead Contact**

Further information and requests for resources and reagents should be directed to and will be fulfilled by the Lead Contact, Galit Alter ([galter@partners.org](mailto:galter@partners.org)).

**Material Availability**

This study did not generate new unique reagents.

**Data and Code Availability Statement**

The dataset generated during and/or analyzed during the current study have been made available in the supplemental material.

**Experimental Model and Subject Details**

### ***Sample set***

Plasma samples from 22 SARS-CoV-2 patients from Seattle were profiled for anti-SARS-CoV-2 antibody responses (**Table 1**). Patients who tested positive for SARS-CoV-2 by real-time reverse-transcriptase–polymerase-chain-reaction (RT-PCR) of a nasopharyngeal swab were enrolled in the study upon hospital admission, and samples after admission were included in this study (**Figure S1**). All enrolled participants gave written, informed consent. The enrolled hospitalized 22 individuals were monitored over the course of their stay, and final outcomes were reported. 12 individuals convalesced and were healthy enough to be discharged, whereas 10 individuals died. Demographic information including age, race, and interventions are summarized across the two groups (**Table 1 and Data S1**).

As a validation cohort, a cohort of 40 individuals from MGH in Boston were enrolled, all participants tested positive for SARS-CoV-2 by RT-PCR and they were monitored over their hospital stay. Samples at time of hospitalization were included in this study. Outcomes were reported as deceased or discharged. Demographics and clinical data for the validation cohort are summarized in Table 2.

All experimental data was performed in two technical and two biological (for primary cell assays) replicates and the average value was used throughout the study. This study was approved by the University of Washington Human Subjects Division Institutional Review Board.

### ***Primary Immune Cells***

Primary immune cells were isolated from fresh peripheral blood from healthy human volunteers collected by the MGH Blood bank or the Ragon institute. The study was approved by the MGH Institutional Review Board. All subjects were over 18 years of age and provided informed consent. All samples were completely de-identified prior to use. Human NK cells and neutrophils isolated from fresh peripheral blood were cultured in RPMI supplemented with 10% fetal bovine serum, L-glutamine, penicillin/streptomycin and maintained at 37°C, 5% CO<sub>2</sub>.

### ***Cell Lines***

THP-1 cells (ATCC) were grown at 37°C, 5% CO<sub>2</sub> in RPMI supplemented with 10% fetal bovine serum, L-glutamine, penicillin/streptomycin and 0.01% b-mercaptoethanol.

### **Methods Details**

#### ***Luminex***

Antigen-specific antibody subclass, isotype, sialic acid, galactose and Fc $\gamma$ -receptor (Fc $\gamma$ R) binding levels were assessed using a 384-well based customized multiplexed Luminex assay, as previously described (Brown et al., 2017). Relative antibody concentration was measured against a panel of SARS-CoV-2 antigens (**Data S1**). SARS-CoV-2 RBD (kindly provided by Aaron Schmidt), SARS-CoV-2 nucleocapsid (N) protein (Aalto Bio Reagents), and SARS-CoV-2 spike protein (S) (kindly provided by Bing Chen) were used to profile the SARS-CoV-2-specific humoral immune response. Briefly, antigens were coupled by covalent NHS-ester linkages via EDC and NHS (Thermo Scientific) to fluorescent carboxyl-modified microspheres (Luminex). Antigen-coupled microspheres were then washed with an automated plate washer (Tecan) and incubated with plasma samples at an appropriate sample dilution (1:500 for IgG1 and all Fc $\gamma$ -receptors, and 1:100 for all other readouts). Detection of antigen-specific antibody titers occurred using a PE-coupled detection antibody for each subclass and isotype (IgG, IgG1, IgG2, IgG3, IgG4, IgA1 and IgM, Southern Biotech), and Fc $\beta$ -receptors were fluorescently labeled with PE before addition to immune complexes (Fc $\gamma$ R2A, 2B, 3A, Duke Protein Production facility). For detection of sialic acid and galactose, fluorescein-labeled plant-based lectin detects, SNA and RCA (Vectorlabs) were added as detection reagents at a 1:100 (SNA) and 1:500 dilution (RCA). Plasma samples were acquired via flow cytometry, using an iQue (Intellicyt) and S-Lab robot (PAA). Analysis was done using ForeCyt software by gating on fluorescent bead regions and PE median fluorescent intensity (MFI) is reported as readout for antigen-specific antibody titers.

#### ***Functional profiling***

For the functional analysis of plasma samples, bead-based assays were used to quantify antibody-dependent cellular phagocytosis (ADCP), antibody-dependent neutrophil phagocytosis (ADNP) and antibody-dependent complement deposition (ADCD), as previously described (Fischinger et al., 2019) (**Data S1**). Fluorescent streptavidin beads (Thermo Fisher) were coupled to biotinylated antigen SARS-CoV-2 RBD, N and S and incubated with diluted plasma (ADCP and ADNP 1:100, ADCD 1:10). For ADCP, THP-1 cells were added to the immune complexes and incubated for 16h at 37°C. For ADNP, primary neutrophils were isolated via negative selection (Stemcell) from whole blood. After 1h incubation at 37°C, neutrophils were stained with an anti-CD66b PacBlue detection antibody (Biolegend). For the ADCD assay, lyophilized guinea pig complement (Cedarlane) was resuspended according to manufacturer's instructions and diluted in gelatin veronal buffer with calcium and magnesium (Boston BioProducts). Post incubation, C3 was detected with Fluorescein-Conjugated Goat IgG Fraction to Guinea Pig Complement C3 (Mpbio).

For detection of antibody-dependent NK cell activity, an ELISA-based approach was used, as described (Boudreau et al., 2020). Briefly, plates were coated with 2 µg/mL of antigen (as mentioned above) and samples were added at a 1:50 dilution and incubated for 2h at 37°C. NK cells were isolated the day prior via RosetteSep (Stem Cell Technologies) from healthy buffy coats and rested overnight in 1 ng/ml IL-15 (Stemcell). NK cells were incubated with immune complexes for 5h at 37°C with a staining cocktail containing CD107a PE-Cy5 (BD), Golgi stop (BD) and Brefeldin A (BFA, Sigma Aldrich). Post NK cell incubation, cells were fixed (Perm A, Life Tech) and stained for surface markers with anti-CD16 APC-Cy7 (BD), anti-CD56 PE-Cy7 (BD) and anti-CD3 PacBlue (BD) while fixing. Post permeabilization with Perm B (Life Tech) and anti-MIP-1 $\beta$  PE (BD) antibodies were used for intracellular staining. All assays were acquired via flow cytometry with an iQue (Intellicyt) and an S-Lab robot (PAA). For ADCP, events were gated on bead-positive cells, whereas neutrophils were defined as CD66b positive followed by gating on bead-positive neutrophils. A phagocytosis score was calculated for ADCP and ADNP as (percentage of bead-positive cells) x (MFI of bead-positive cells) divided by 10000. ADCC was reported as MFI of C3 deposition. NK cells were defined as CD3-, CD16+ and CD56+. Data were reported as percentage of cells positive for CD107a or MIP-1 $\beta$ .

#### ***Pseudovirus Neutralization Antibody Assay***

The 2019-nCoV pseudoviruses expressing a luciferase reporter gene were generated as described previously (**Data S1**) (Yang et al., 2004). Briefly, the packaging construct psPAX2 (Cat# 11348, AIDS Reagent), luciferase reporter plasmid pLenti-CMV Puro-Luc (Cat# 17447, Addgene) and Spike protein expressing pcDNA3.1-SARS CoV-2.SACT were co-transfected into HEK293T cells at ratio of 1:1:0.5 by Calcium phosphate transfection method. The supernatants containing the pseudotype viruses were collected 48 hours post-transfection and filtered by 0.45-µm filter. The viruses were stored at -80°C freezer till use. To determine the neutralization activity of the antisera from vaccinated animals, HEK293T cells were firstly transfected with pcDNA3.1(-)-hACE2 (Cat# 1786, Addgene). 12 hours post transfection; the HEK293T/hACE2 cells were seeded at 96-well tissue culture plate at density of 2.00E+04 cells/well overnight. Heat (56°C, 30 min) inactivated antisera were twofold serial diluted and mixed with 50µl of pseudoviruses. The mixture was incubated at 37°C incubator for 1 hour before adding into HEK293T/hACE2 cells in 96-well plates. Six hours after infection, the cell culture medium was replenished with fresh DMEM (supplemented with 2% FBS). Forty-eight hours after infection, cells were lysed in Steady-Glo Luciferase Assay (Promega). A standard quantity of cell lysate was used in a luciferase assay with luciferase assay reagent (Promega) according to the manufacturer's protocol.

## Quantification and Statistical Analysis

All analyses were performed using python version 3.6.8 with statistical and machine learning packages (Pedregosa et al., 2011). Networks were visualized in Cytoscape. Raw data are available in supplementary information.

### ***Classification of Convalescent and Deceased Groups***

The classification models were trained to distinguish convalescent and deceased groups with a minimal set of features, to avoid overfitting. PBS controls was subtracted from all features, Fc array features were log transformed, and all data was scaled and centered. Antibody features including sex and interventions (**Table 1**) were included the selection process, and covariates were binarized and scaled and center prior to analysis.

The models were built using a backward feature elimination for selection and then classified using the minimal set of features which maximize accuracy (Guyon and Elisseeff, 2003; Pittala et al., 2019). Models were trained and tested in a fivefold cross-validation framework using random stratified sampling to ensure that both groups are represented in each group. Within each fold, samples were further subdivided into four sets for each iterative fold-specific elimination. A partial least squares discriminant analysis (PLS) classifier was then trained using the fold-specific selected features to predict the test set. Multiple iterations of fold specific feature selections were performed to obtain a single model. This process was repeated over twenty replicates and convergent correlates were observed (Ackerman et al., 2018).

Performance and robustness of the model was contrasted with negative control models constructed from permuted data and randomly selected size-matched features, with multiple iterations of fivefold cross-validation used to generate classification accuracies. These control models were generated 100 times. The permuted control was generated in the same process as above shuffling labels randomly for each repetition. Size-matched features were chosen at random for each cross-validation step within each repetition. Predicted and true outcomes were compared to determine accuracy. Robustness was defined as the effect size of the distributions (Cliff's  $\Delta$ ), and the exact P values of the tail probabilities of the true distributions within the control distributions. Reported are the median p-values across twenty independent cross-validation replicates (Ojala and Garriga, 2010).

### ***Correlation Networks***

Correlation networks were constructed to visualize the additional humoral immune features that were significantly linked to the selected minimal biomarkers, to provide enhanced insights into the biological mechanisms by which antibodies may provide protection following infection. In brief, antibody features that were significantly correlated with a Holms-Bonferroni correction to the final selected PLS model selected-features were defined as co-correlates. Significant spearman correlations above a threshold of  $|r| > 0.5$  were visualized within the networks.

### ***Sensitivity Analysis***

Using the selected features from the original model a new PLSDA model was trained excluding a single outlier at a time in a fivefold cross validation framework. This process was repeated three times, each time generating a unique ROC curve as the top 3 individual outliers were removed. Using these cross validated ROC curves the mean performance and variation were assessed and are summarized as area under curve.

### ***Ratio Based Analyses***

In order to evaluate S vs N ratios, first ratios for each feature were defined separately by simply dividing S-responses over N-responses for every given feature. S:N ratios were visualized by log2 transformation for ease of interpretation. Differences across convalescents and deceased were then tested with a one-sided Mann-Whitney U test and a Holm-Bonferroni multiple hypothesis correction criterion.

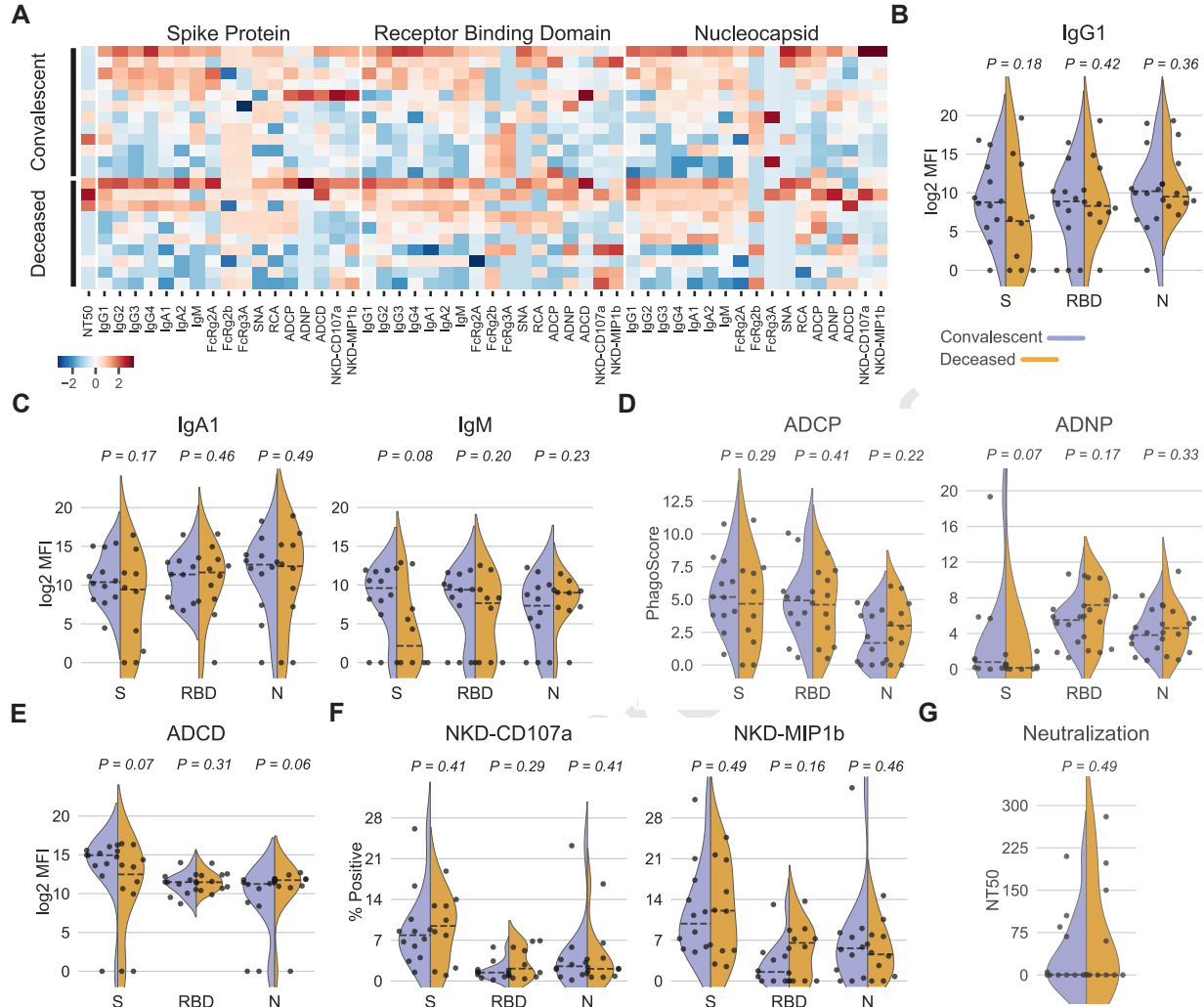
In order to address whether the overall S-response was enriched over N-responses in the convalescents across all features tested, all data was background corrected and z-score normalized. Then the number of S-features which were greater than their N-counterparts across every feature were summed. This analysis yielded a distribution of individual S greater than N scores for each group and statistical differences were assessed using a one-sided Mann-Whitney U test.

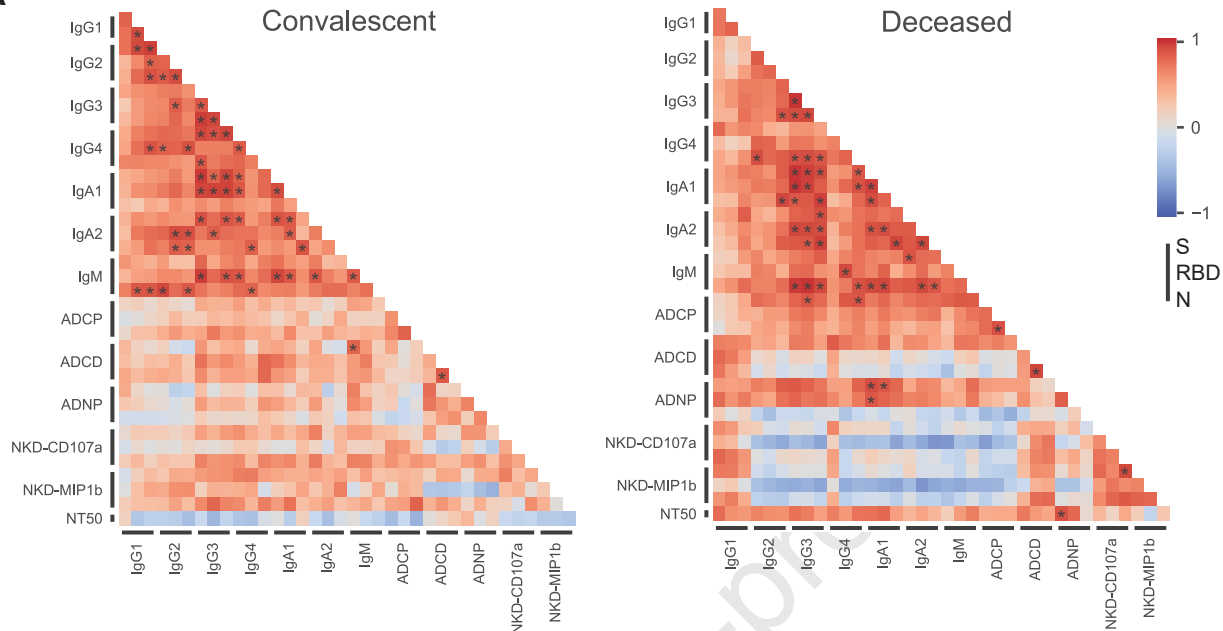
**References:**

- Ackerman, M.E., Das, J., Pittala, S., Broge, T., Linde, C., Suscovich, T.J., Brown, E.P., Bradley, T., Natarajan, H., Lin, S., *et al.* (2018). Route of immunization defines multiple mechanisms of vaccine-mediated protection against SIV. *Nat Med* 24, 1590-1598.
- Amanat, F., Stadlbauer, D., Strohmeier, S., Nguyen, T.H.O., Chromikova, V., McMahon, M., Jiang, K., Arunkumar, G.A., Jurczyszak, D., Polanco, J., *et al.* (2020). A serological assay to detect SARS-CoV-2 seroconversion in humans. *Nat Med*.
- Ayala-Nunez, N.V., Hoornweg, T.E., van de Pol, D.P., Sjollema, K.A., Flipse, J., van der Schaer, H.M., and Smit, J.M. (2016). How antibodies alter the cell entry pathway of dengue virus particles in macrophages. *Sci Rep* 6, 28768.
- Bar-On, Y.M., Flamholz, A., Phillips, R., and Milo, R. (2020). SARS-CoV-2 (COVID-19) by the numbers. *Elife* 9.
- Barouch, D.H., Alter, G., Broge, T., Linde, C., Ackerman, M.E., Brown, E.P., Borducchi, E.N., Smith, K.M., Nkolola, J.P., Liu, J., *et al.* (2015). Protective efficacy of adenovirus/protein vaccines against SIV challenges in rhesus monkeys. *Science* 349, 320-324.
- Bhatraju, P.K., Ghassemieh, B.J., Nichols, M., Kim, R., Jerome, K.R., Nalla, A.K., Greninger, A.L., Pipavath, S., Wurfel, M.M., Evans, L., *et al.* (2020). Covid-19 in Critically Ill Patients in the Seattle Region - Case Series. *N Engl J Med*.
- Boudreau, C.M., Yu, W.H., Suscovich, T.J., Talbot, H.K., Edwards, K.M., and Alter, G. (2020). Selective induction of antibody effector functional responses using MF59-adjuvanted vaccination. *J Clin Invest* 130, 662-672.
- Brown, E.P., Dowell, K.G., Boesch, A.W., Normandin, E., Mahan, A.E., Chu, T., Barouch, D.H., Bailey-Kellogg, C., Alter, G., and Ackerman, M.E. (2017). Multiplexed Fc array for evaluation of antigen-specific antibody effector profiles. *J Immunol Methods* 443, 33-44.
- Buchholz, U.J., Bukreyev, A., Yang, L., Lamirande, E.W., Murphy, B.R., Subbarao, K., and Collins, P.L. (2004). Contributions of the structural proteins of severe acute respiratory syndrome coronavirus to protective immunity. *Proc Natl Acad Sci U S A* 101, 9804-9809.
- Chandrashekhar, A., Liu, J., Martinot, A.J., McMahan, K., Mercado, N.B., Peter, L., Tostanoski, L.H., Yu, J., Maliga, Z., Nekorchuk, M., *et al.* (2020). SARS-CoV-2 infection protects against rechallenge in rhesus macaques. *Science*.
- Chang, S.C., Wang, J.T., Huang, L.M., Chen, Y.C., Fang, C.T., Sheng, W.H., Wang, J.L., Yu, C.J., and Yang, P.C. (2005). Longitudinal analysis of Severe Acute Respiratory Syndrome (SARS) coronavirus-specific antibody in SARS patients. *Clin Diagn Lab Immunol* 12, 1455-1457.
- Chen, G., Wu, D., Guo, W., Cao, Y., Huang, D., Wang, H., Wang, T., Zhang, X., Chen, H., Yu, H., *et al.* (2020). Clinical and immunological features of severe and moderate coronavirus disease 2019. *J Clin Invest*.
- Chung, A.W., Ghebremichael, M., Robinson, H., Brown, E., Choi, I., Lane, S., Dugast, A.S., Schoen, M.K., Rolland, M., Suscovich, T.J., *et al.* (2014). Polyfunctional Fc-effector profiles mediated by IgG subclass selection distinguish RV144 and VAX003 vaccines. *Sci Transl Med* 6, 228ra238.
- Cobey, S., and Hensley, S.E. (2017). Immune history and influenza virus susceptibility. *Curr Opin Virol* 22, 105-111.
- de Wit, E., van Doremalen, N., Falzarano, D., and Munster, V.J. (2016). SARS and MERS: recent insights into emerging coronaviruses. *Nat Rev Microbiol* 14, 523-534.
- DiLillo, D.J., Palese, P., Wilson, P.C., and Ravetch, J.V. (2016). Broadly neutralizing anti-influenza antibodies require Fc receptor engagement for in vivo protection. *J Clin Invest* 126, 605-610.

- Fischinger, S., Fallon, J.K., Michell, A.R., Broge, T., Suscovich, T.J., Streeck, H., and Alter, G. (2019). A high-throughput, bead-based, antigen-specific assay to assess the ability of antibodies to induce complement activation. *J Immunol Methods* 473, 112630.
- Gunn, B.M., and Alter, G. (2016). Modulating Antibody Functionality in Infectious Disease and Vaccination. *Trends Mol Med* 22, 969-982.
- Guyon, I., and Elisseeff, A. (2003). An Introduction to Variable and Feature Selection. *Journal of Machine Learning Research* 3, 1157-1182
- Hauser, Anthony et al. 2020. "Estimation of SARS-CoV-2 Mortality during the Early Stages of an Epidemic: A Modelling Study in Hubei, China and Northern Italy." *medRxiv*.
- He, Y., Li, J., and Jiang, S. (2006). A single amino acid substitution (R441A) in the receptor-binding domain of SARS coronavirus spike protein disrupts the antigenic structure and binding activity. *Biochem Biophys Res Commun* 344, 106-113.
- Holshue, M.L., DeBolt, C., Lindquist, S., Lofy, K.H., Wiesman, J., Bruce, H., Spitters, C., Ericson, K., Wilkerson, S., Tural, A., et al. (2020). First Case of 2019 Novel Coronavirus in the United States. *N Engl J Med* 382, 929-936.
- Lau, K.S., Juchheim, A.M., Cavaliere, K.R., Philips, S.R., Lauffenburger, D.A., and Haigis, K.M. (2011). In vivo systems analysis identifies spatial and temporal aspects of the modulation of TNF-alpha-induced apoptosis and proliferation by MAPKs. *Sci Signal* 4, ra16.
- Li, R., Pei, S., Chen, B., Song, Y., Zhang, T., Yang, W., and Shaman, J. (2020). Substantial undocumented infection facilitates the rapid dissemination of novel coronavirus (SARS-CoV2). *Science*.
- Li, T., Xie, J., He, Y., Fan, H., Baril, L., Qiu, Z., Han, Y., Xu, W., Zhang, W., You, H., et al. (2006). Long-term persistence of robust antibody and cytotoxic T cell responses in recovered patients infected with SARS coronavirus. *PLoS One* 1, e24.
- Liu, W., Liu, L., Kou, G., Zheng, Y., Ding, Y., Ni, W., Wang, Q., Tan, L., Wu, W., Tang, S., et al. (2020). Evaluation of Nucleocapsid and Spike Protein-based ELISAs for detecting antibodies against SARS-CoV-2. *J Clin Microbiol*.
- Ojala, M., and Garriga, G. (2010). Permutation tests for studying classifier performance. *Journal of Machine Learning Research* 11, 1833-1863.
- Pittala, S., Bagley, K., Schwartz, J.A., Brown, E.P., Weiner, J.A., Prado, I.J., Zhang, W., Xu, R., Ota-Setlik, A., Pal, R., et al. (2019). Antibody Fab-Fc properties outperform titer in predictive models of SIV vaccine-induced protection. *Mol Syst Biol* 15, e8747.
- Quinlan, B.D., Mou, H., Zhang, L., Guo, Y., He, W., Ojha, A., Parcells, M.S., Luo, G., Li, W., Zhong, G., et al. (2020). The SARS-CoV-2 receptor-binding domain elicits a potent neutralizing response without antibody-dependent enhancement. *bioRxiv*, 2020.2004.2010.036418.
- Saphire, E.O., Schendel, S.L., Gunn, B.M., Milligan, J.C., and Alter, G. (2018). Antibody-mediated protection against Ebola virus. *Nat Immunol* 19, 1169-1178.
- Shi, Y., Wan, Z., Li, L., Li, P., Li, C., Ma, Q., and Cao, C. (2004). Antibody responses against SARS-coronavirus and its nucleocapsid in SARS patients. *J Clin Virol* 31, 66-68.
- ter Meulen, J., van den Brink, E.N., Poon, L.L., Marissen, W.E., Leung, C.S., Cox, F., Cheung, C.Y., Bakker, A.Q., Bogaards, J.A., van Deventer, E., et al. (2006). Human monoclonal antibody combination against SARS coronavirus: synergy and coverage of escape mutants. *PLoS Med* 3, e237.
- Timani, K.A., Ye, L., Ye, L., Zhu, Y., Wu, Z., and Gong, Z. (2004). Cloning, sequencing, expression, and purification of SARS-associated coronavirus nucleocapsid protein for serodiagnosis of SARS. *J Clin Virol* 30, 309-312.
- Tomaras, G.D., and Haynes, B.F. (2009). HIV-1-specific antibody responses during acute and chronic HIV-1 infection. *Curr Opin HIV AIDS* 4, 373-379.
- WHO (2020). Coronavirus disease (COVID-19) Situation Report - 122.

- Wu, F., Wang, A., Liu, M., Wang, Q., Chen, J., Xia, S., Ling, Y., Zhang, Y., Xun, J., Lu, L., et al. (2020a). Neutralizing antibody responses to SARS-CoV-2 in a COVID-19 recovered patient cohort and their implications. *medRxiv*, 2020.2003.2030.20047365.
- Wu, F., Zhao, S., Yu, B., Chen, Y.M., Wang, W., Song, Z.G., Hu, Y., Tao, Z.W., Tian, J.H., Pei, Y.Y., et al. (2020b). A new coronavirus associated with human respiratory disease in China. *Nature* 579, 265-269.
- Yang, Z.Y., Kong, W.P., Huang, Y., Roberts, A., Murphy, B.R., Subbarao, K., and Nabel, G.J. (2004). A DNA vaccine induces SARS coronavirus neutralization and protective immunity in mice. *Nature* 428, 561-564.
- Yasui, F., et al. (2014). Phagocytic cells contribute to the antibody-mediated elimination of pulmonary-infected SARS coronavirus. *Virology*
- Yu, J., Tostanoski, L.H., Peter, L., Mercado, N.B., McMahan, K., Mahrokhan, S.H., Nkolola, J.P., Liu, J., Li, Z., Chandrashekhar, A., et al. (2020). DNA vaccine protection against SARS-CoV-2 in rhesus macaques. *Science*.
- Zhao, J., Perera, R.A., Kayali, G., Meyerholz, D., Perlman, S., and Peiris, M. (2015). Passive immunotherapy with dromedary immune serum in an experimental animal model for Middle East respiratory syndrome coronavirus infection. *J Virol* 89, 6117-6120.
- Zhao, Y., Wang, C., Qiu, B., Li, C., Wang, H., Jin, H., Gai, W., Zheng, X., Wang, T., Sun, W., et al. (2017). Passive immunotherapy for Middle East Respiratory Syndrome coronavirus infection with equine immunoglobulin or immunoglobulin fragments in a mouse model. *Antiviral Res* 137, 125-130.
- Zhu, N., Zhang, D., Wang, W., Li, X., Yang, B., Song, J., Zhao, X., Huang, B., Shi, W., Lu, R., et al. (2020). A Novel Coronavirus from Patients with Pneumonia in China, 2019. *N Engl J Med* 382, 727-733.
- CONG, J. & WEI, H. 2019. Natural Killer Cells in the Lungs. *Front Immunol*, 10, 1416. JEGASKANDA, S., LUKE, C., HICKMAN, H. D., SANGSTER, M. Y., WIELAND-ALTER, W. F., MCBRIDE, J. M., YEWDELL, J. W., WRIGHT, P. F., TREANOR, J., ROSENBERGER, C. M. & SUBBARAO, K. 2016. Generation and Protective Ability of Influenza Virus-Specific Antibody-Dependent Cellular Cytotoxicity in Humans Elicited by Vaccination, Natural Infection, and Experimental Challenge. *J Infect Dis*, 214, 945-52.
- LU, L. L., CHUNG, A. W., ROSEBROCK, T. R., GHEBREMICHAEL, M., YU, W. H., GRACE, P. S., SCHOEN, M. K., TAFESSE, F., MARTIN, C., LEUNG, V., MAHAN, A. E., SIPS, M., KUMAR, M. P., TEDESCO, J., ROBINSON, H., TKACHENKO, E., DRAGHI, M., FREEDBERG, K. J., STREECK, H., SUSCOVICH, T. J., LAUFFENBURGER, D. A., RESTREPO, B. I., DAY, C., FORTUNE, S. M. & ALTER, G. 2016. A Functional Role for Antibodies in Tuberculosis. *Cell*, 167, 433-443 e14.
- VAN ERP, E. A., LUYTJES, W., FERWERDA, G. & VAN KASTEREN, P. B. 2019. Fc-Mediated Antibody Effector Functions During Respiratory Syncytial Virus Infection and Disease. *Front Immunol*, 10, 548.
- WANG, X., GUO, X., XIN, Q., PAN, Y., LI, J., CHU, Y., FENG, Y. & WANG, Q. 2020. Neutralizing Antibodies Responses to SARS-CoV-2 in COVID-19 Inpatients and Convalescent Patients. *medRxiv*, 2020.04.15.20065623.
- Pedregosa, Fabian, Gaël Varoquaux, Alexandre Gramfort, Vincent Michel, Bertrand Thirion, Olivier Grisel, Mathieu Blondel, et al. "Scikit-Learn: Machine Learning in Python." *Journal of Machine Learning Research* 12, no. 85 (2011): 2825–30.



**A****B**